

# Jefferson Lab PAC 25 Proposal Cover Sheet

This document must  
be received by close  
of business Tuesday,

December 2, 2003 at:

Jefferson Lab  
User/International Liaison  
Mail Stop 12B  
12000 Jefferson Ave.  
Newport News, VA  
23606

Experimental Hall: B

Days Requested for Approval: NONE (LOI)

**Proposal Title:**

Two-Photon Exchange from a Precise Comparison  
of e+p and e-p Elastic Scattering in CLAS

**Proposal Physics Goals**

Indicate any experiments that have physics goals similar to those in your proposal.

**Approved, Conditionally Approved, and/or Deferred Experiment(s) or proposals:****Contact Person**

**Name:** Will Brooks

**Institution:** Jefferson Lab

**Address:**

**Address:**

**City, State, ZIP/ Country:**

**Phone:** 757-269-6391

**Fax:** 757-269-5800

**E-Mail:** brooksw@jlab.org

Jefferson Lab Use Only

Receipt Date: \_\_\_\_\_

By: \_\_\_\_\_

# Two-Photon Exchange from a Precise Comparison of $e^+p$ and $e^-p$ Elastic Scattering in CLAS

A Letter of Intent to PAC 25

K. Joo

*University of Connecticut*

F. Klein

*The Catholic University of America*

B. A. Raue

*Florida International University*

A. Afanasev, W. K. Brooks, V. D. Burkert,  
L. Elouadrhiri, B. A. Mecking

*Jefferson Lab*

L. B. Weinstein

*Old Dominion University*

## Abstract

A direct measurement of the two photon exchange contribution to lepton-proton elastic scattering is proposed. This process has been suggested to play an important role in explaining the discrepancy observed in measuring the proton's  $G_E/G_M$  ratio in two different approaches. A definitive test of this assertion is possible via a high precision comparison of  $e^+p$  and  $e^-p$  elastic scattering. The proposed measurement, which uniquely exploits the large acceptance of CLAS, may also influence the interpretation of other measurements involving small amplitudes, such as parity violation experiments, or determining the small amplitudes in the  $N$  to  $\Delta$  transition.

## 1 Introduction

The electromagnetic form factors are essential pieces of our knowledge of nucleon structure. However, the proton electric form factor,  $G_E^p$ , is currently unknown by a factor of five at  $Q^2 = 6 \text{ GeV}^2$ .<sup>[1, 2, 3, 4, 5]</sup> This causes grave uncertainties for both theoretical and experimental physics. Theoretically, it is unclear what value of  $G_E^p$  should be used to compare to models of proton structure (eg: lattice calculations). Experimentally, it is unclear what value of  $G_E^p$  should be used to interpret experiments from  $(e, e'p)$  through color transparency.

This uncertainty arises from a discrepancy between Rosenbluth separations of the unpolarized cross section [1, 4, 5] and polarization transfer measurements [2, 3]. Assuming one photon exchange (first Born approximation), the cross section can be written as

$$d\sigma_B = C_B(Q^2, \epsilon) \left[ \tau G_M^2(Q^2) + \epsilon G_E^2(Q^2) \right]$$

where the virtual photon polarization  $\epsilon = [1 + 2(1 + \tau) \tan^2(\theta_e/2)]^{-1}$ ,  $\tau = Q^2/4M^2$  and  $C_B$  is a known kinematic factor. By varying  $\epsilon$ , the Rosenbluth measurements separate  $R_L$ , which is proportional to  $G_E^{p,2}$ , from  $R_T$ , which depends on both  $G_E^p$  and  $G_M^p$ . In  $(\vec{e}, e'\vec{p})$  in Born approximation, the ratio of the transverse and longitudinal recoil proton polarization  $P_t/P_l$  is directly proportional to  $G_E^p/G_M^p$ . Recent “Super-Rosenbluth” measurements, where the recoil proton (rather than the scattered electron) was detected have confirmed the original Rosenbluth measurements with much smaller systematic uncertainties.

The most likely cause of this discrepancy is the unwarranted assumption of one photon exchange approximation. The contribution of the proton electric form factor,  $G_E^p$ , to the Rosenbluth cross section is kinematically suppressed (compared to the magnetic form factor,  $G_M^p$ ) for 4-momentum transfers,  $Q^2 \geq 2 \text{ GeV}^2$ . Therefore a small (5–10%)  $\epsilon$ -dependent Two-Photon-Exchange (TPE) correction to the dominant magnetic term could drastically change the apparent value of  $G_E^p$  obtained from a Rosenbluth separation. It could simulate a contribution of the electric form factor of the form  $G_E^p \mu_p / G_M^p = 1$  even if  $G_E^p$  is actually the totally different dependence obtained from polarization transfer data. Note that in order to affect the Rosenbluth separation measurement, the above correction should have a strong  $\epsilon$ -dependence.

Guichon and Vanderhaeghen [6] parameterized the two-photon exchange (TPE) amplitude in the most general form and fitted the discrepancy between polarization transfer and Rosenbluth measurements in order to evaluate the magnitude of the TPE effect. They discussed the possible angular dependence of the correction and concluded that the TPE effect is up to about 3.5% at the amplitude level. Blunden, Melnitchouk and Tjon, [7] calculated the elastic nucleon contribution to the TPE effect and found that it accounts for almost half of the difference between the Rosenbluth and polarization measurements. Afanasev, Brodsky and Carlson [8] calculated the TPE effects at the quark-parton level and obtained a few percent effect from the short-range electron-quark interaction. The results from both the models and the fits are mostly  $Q^2$  independent. The magnitude of the expected cross section change at  $\epsilon = 0.2$  ranges from 1 to 7%.

Note that these TPE effects are different from other higher order effects that are considered a ‘standard’ radiative correction and already applied to the cross section data as a part of data analysis procedure [9]. They include soft photon bremsstrahlung, vertex corrections and vacuum polarization. They also include TPE effects calculated in the limit when almost the entire momentum is carried by one of the photons, while the second photon is soft. Such corrections are often called ‘model independent’, since in this case the entire dynamics of electron-nucleon interaction can be described only by two elastic form factors of one-photon exchange approximation.

The few-percent TPE effects, referred to as ‘dispersive effects,’ have been seen before in electron scattering on heavier nuclei. They showed up typically in the energy dependence of form factors measured in elastic electron scattering [10] and in discrepancies between nuclear charge radii measured with

muonic atoms and with elastic electron scattering [11]. They were studied in several different ways, including ‘forbidden transitions’ in electron scattering (eg:  $^{16}\text{O}(e, e') 0^+ \rightarrow 0^-$ (10.9) MeV[12]), and the comparison of electron and positron elastic scattering from  $^{12}\text{C}$  [13]. However, it was generally assumed that these few-percent effects would be much smaller on the proton ( $Z = 1$ ) than on real nuclei ( $Z \gg 1$ ).

Since two-photon exchange can potentially have a huge effect on  $G_E^p$ , an experimental determination of its contribution becomes very important. The most straightforward way to measure these effects is to compare the cross section measured with electrons and with positrons. Two-photon exchange would enter with an opposite sign, doubling the magnitude of the effect (see the Scientific Motivation section for details).

Arrington [14] reanalyzed historical electron-proton and positron-proton elastic scattering data to find indications that the  $e^+/e^-$  cross section ratio at  $Q^2 > 1 \text{ GeV}^2$  and small  $\epsilon$  is about 1.04. However, there are only seven data points at  $\epsilon < 0.5$  and only one of those is at  $Q^2 > 1 \text{ GeV}^2$ . In addition, the statistical errors are typically at least 5%.

We propose to measure the  $e^+/e^-$  cross section ratio with high statistical precision. We will use a 5.5 GeV electron beam incident on the CLAS tagger to create a real photon beam. The photon beam will strike a converter, creating  $e^+/e^-$  pairs. The electrons and positrons will be separated from the photon beam by a dipole magnet. They will then strike two separated hydrogen targets (with the photon beam passing between the targets). We will then detect the recoil protons and the scattered leptons in the CLAS spectrometer. In order to reduce systematic errors, we will periodically flip the polarity of the  $e^+/e^-$  separator magnet and of the CLAS toroidal magnet. By doing this, we will simultaneously measure the cross section for  $e^+$  and  $e^-$  scattering from the proton to determine the magnitude of two-photon exchange effects with high statistical and systematic precision.

These measurements will help us determine the effects of TPE on electron-proton elastic scattering and resolve the ambiguity presently surrounding the charge form factor of the proton.

Section 2 will discuss the theoretical considerations in more detail and section 3 will present the experimental method.

## 2 Scientific Motivation

The Rosenbluth formula for elastic  $ep$ -scattering [15] was derived using the one-photon exchange approximation. Measurements of nucleon electromagnetic form factors and experiments on parity-violating electron scattering are based on the same approximation. When electron scattering data are analysed, radiative corrections (RC) must be taken into account. A procedure of applying RC to experimentally measured observables is based on QED, and the technique developed by Mo and Tsai [9] is commonly used in this case. More recent calculations include such effects as finite nucleon size [16] and hard nonfactorizable bremsstrahlung [17], the latter being essential for polarization observables.

Because of logarithmic enhancements of the type  $\log(Q^2/m_e^2)$ , the magnitude of RC may reach tens of percent. At the same time, the Rosenbluth technique for measurements of the electric nucleon form factor aims at separating the 5-10% electric contribution from the measured cross section. Therefore precise knowledge of RC is of paramount importance in this case. While RC associated with photon emission/absorption by electrons can be predicted with high accuracy, the loop corrections of the type shown in Fig.1 introduce uncertainties at a few percent level. Direct measurements of such corrections will therefore allow unambiguous interpretation of electron-proton scattering measurements with an accuracy better than 1%.

Fortunately, the contribution of TPE mechanism Fig. 1 can be measured directly without referring to models of nucleon structure. This is possible due to the fact that the TPE correction has opposite signs for scattering cross sections of positrons vs. electrons, producing a measurable charge asymmetry such as

$$R = \frac{\sigma(e^+)}{\sigma(e^-)} - 1, \quad (1)$$

where  $\sigma(e^+)$  and  $\sigma(e^-)$  denote elastic cross sections of positron- and electron-proton scattering, respectively.

Let us demonstrate the relation of the charge asymmetry in Eq. 1 to the TPE correction to the cross section. The amplitude of elastic  $ep$ -scattering with the accuracy of  $\alpha_{em}^2$  can be written as

$$A_{ep \rightarrow ep} = e_e Z A_{Born} + e_e^2 Z A_{e.br.} + e_e Z^2 A_{p.br.} + e_e^2 Z^2 A_{2\gamma}, \quad (2)$$

where the electron ( $e_e$ ) and target ( $Z=1$  for the proton) charges are written

explicitly, and the amplitudes  $A_{Born}$ ,  $A_{e.br.}$ ,  $A_{p.br.}$  and  $A_{2\gamma}$  respectively describe one-photon exchange, electron bremsstrahlung, proton bremsstrahlung and two-photon exchange. Note that RC such as vertex corrections and vacuum polarization do not lead to the charge asymmetry and therefore are not included here. Squaring the amplitude in Eq. 2 and keeping the corrections up to the order  $\alpha_{em}$  that have odd powers of electron charge, we have

$$|A_{ep \rightarrow ep}|^2 = e_e^2 Z^2 [|A_{Born}|^2 + e_e Z A_{Born} 2 \operatorname{Re}(A_{2\gamma}^*) + e_e Z 2 \operatorname{Re}(A_{e.br.} A_{p.br.}^*)], \quad (3)$$

where the notation  $\operatorname{Re}$  is used for the real part of the amplitude.

Corrections that have an even power of electron charge, including the largest correction from electron bremsstrahlung, do not lead to charge asymmetry. The last term in the above expression describes interference between electron and proton bremsstrahlung. Its infrared divergence exactly cancels the corresponding infrared divergence of the term  $A_{Born} \operatorname{Re}(A_{2\gamma}^*)$ , making the QED description of the ep-scattering self-consistent. This interference effect for the standard kinematics of elastic ep-scattering experiments is dominated by soft-photon emission and results in a factorizable correction already included in the standard approach to RC [9].

Therefore the TPE radiative correction  $\delta$  to the electron scattering cross section that leads to charge asymmetry can be written as

$$\sigma = \sigma_{Born} (1 + e_e Z \delta_{2\gamma}), \quad (4)$$

where  $\delta_{2\gamma}$  is a TPE correction. It translates to the charge asymmetry in Eq. 1 as follows:

$$R = \frac{\sigma(e^+)}{\sigma(e^-)} - 1 = -2e_e Z \delta_{2\gamma}. \quad (5)$$

Thus it is evident that the charge asymmetry of Eq. 1 is a direct and model-independent measure of the TPE effect for the elastic electron-proton scattering.

Figures 2 and 3 show the early SLAC data on charge asymmetry [18] plotted against two model predictions. One model labeled ‘Axial-VMD’ was originally proposed by Drell and Sullivan [19] and recently revised by Afanasev [8]. In this model, the entire strength of the TPE effect is attributed to exchanges of axial mesons such as  $a_1(1260)$  and  $f_1(1285)$ , which are the lightest mesons whose coupling conserves electron helicity and has positive charge parity of the 2-photon exchange. The axial meson coupling was obtained from the fit to the difference between Rosenbluth and polarization

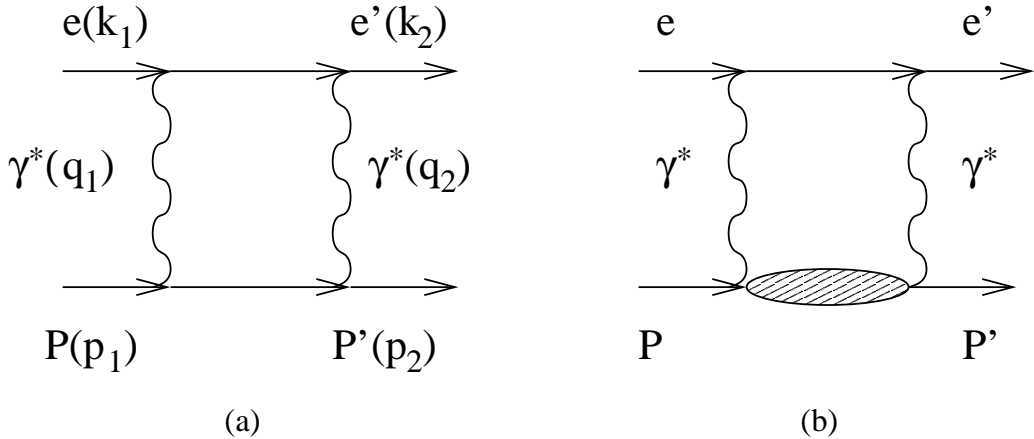


Figure 1: Representative Feynman diagrams for the two-photon exchange in elastic  $ep$ -scattering. Diagrams with crossed photon lines are not shown. a) Elastic intermediate state. b) Inelastic intermediate states, *e.g.*, nucleon resonances and nucleon+mesons.

measurements of the ratio  $G_E^p/G_M^p$ . The second model prediction is a calculation at the quark-parton level in the double logarithm approximation [8]. Like the axial-VMD fit, it brings Rosenbluth and polarization data on  $G_E^p$  into qualitative agreement, but its dependence on the electron scattering angle (or  $\epsilon$ ) at fixed  $Q^2$  is rather different.

Therefore the proposed measurement, besides giving a definite answer to the problem of discrepancy between Rosenbluth and polarization data, will also constrain the models of TPE effect that depend on the nucleon structure.

### 3 Experimental Method

The following sections contain a discussion of the experimental equipment, triggering and data analysis, systematic errors, and rate estimates.

## Charge Asymmetry for Elastic $e^{+/-} p$ Scattering

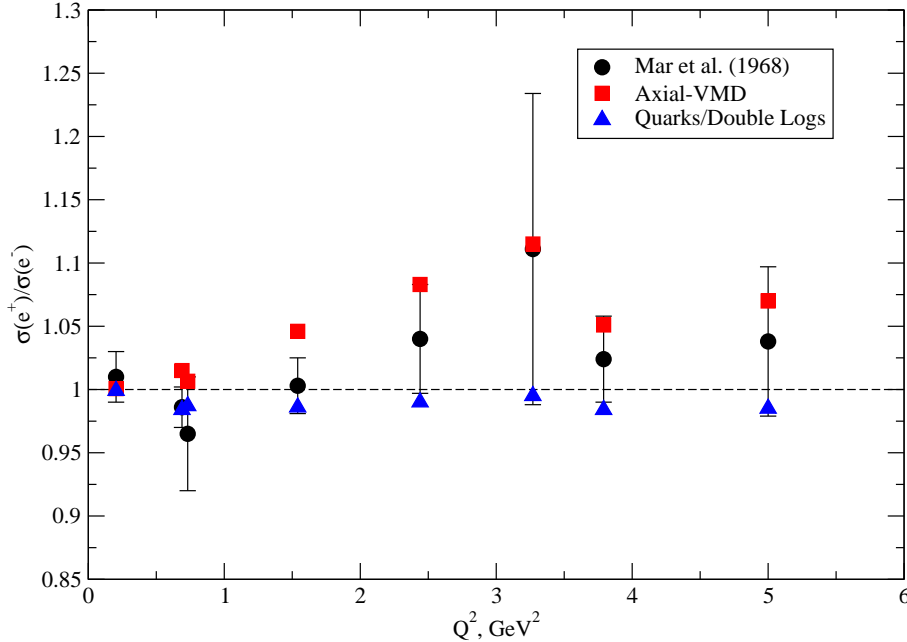


Figure 2: The ratio of the  $e^+ p$  differential cross section to the  $e^- p$  differential cross section as a function of  $Q^2$ .

### 3.1 Description of experimental equipment

The measurement is to be carried out using the CEBAF Large Acceptance Spectrometer, CLAS, in Hall B. The spectrometer and triggering system are all to be used in their standard configurations, however, several beamline devices will be customized for this experiment to provide the positron and electron beams. Portions of the bremsstrahlung tagger will be used as well, but the tagging detectors and electronics will be turned off.

A schematic drawing of the beamline is shown in Fig. 4. The electron beam from the accelerator impinges on the radiator located in the conventional position in front of the tagger magnet, and this magnet will be energized to deflect the primary beam to the tagger dump. The photon beam propagates along the beamline axis, passing through a large-aperture colli-

## Charge Asymmetry for Elastic $e^{+/-} p$ Scattering

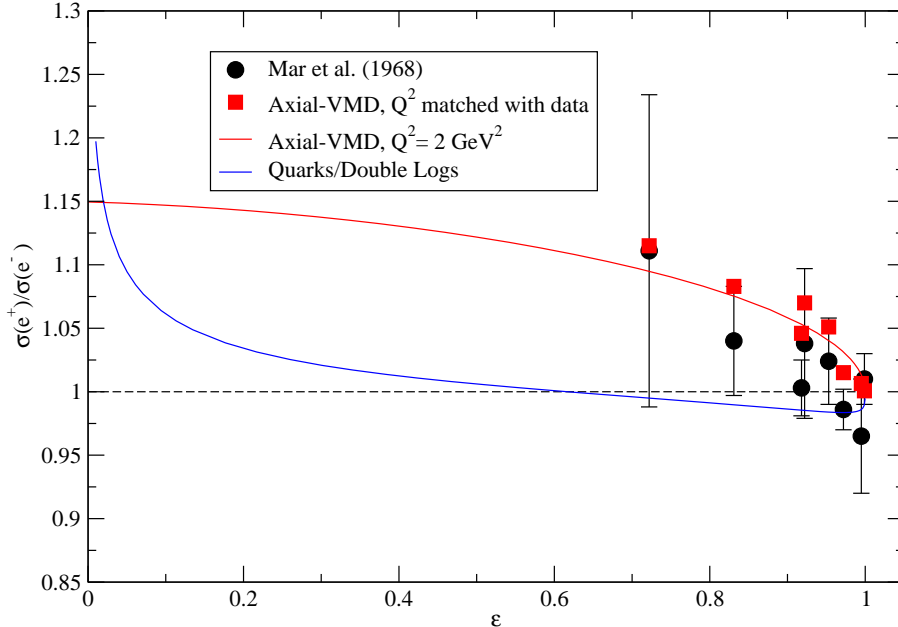


Figure 3: The ratio of the  $e^+ p$  differential cross section to the  $e^- p$  differential cross section as a function of  $\epsilon$ .

mator and a sweeping magnet. The initial beam energy has been chosen to be large so that the natural divergence of the photon beam is small, therefore, minimal collimation is needed. The collimated photon beam then passes through a converter, producing electron-positron pairs. These pairs are separated by a dipole separator magnet with a small field that is sufficient to just separate the positrons and electrons from the photon beam. The low energy tail of the resulting positron and electron beam is stopped by edge block shielding, and the remaining secondary beams then propagate to two cryogenic liquid hydrogen targets, where they can interact. Low-energy particles from edge scattering and Moller scattering can be shielded by the minitorus magnet in its standard configuration; depending on the rates, this may not be necessary.

An illustration from a GEANT simulation is shown in Fig. 5. This is a

# Schematic – top view

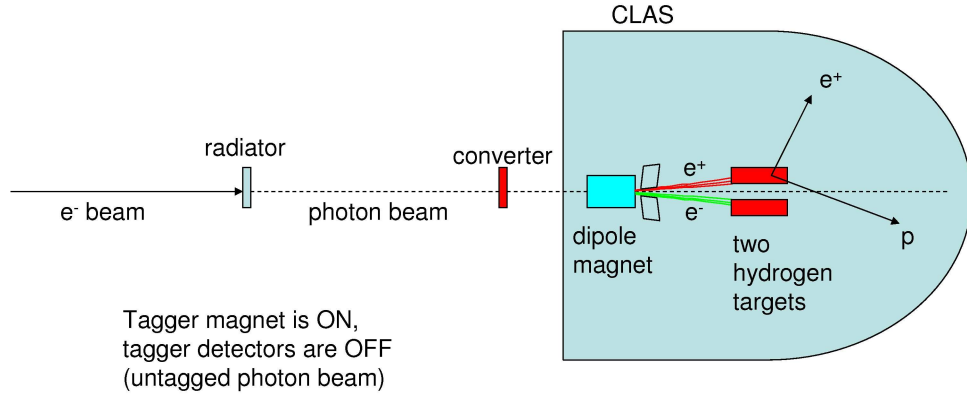


Figure 4: A schematic drawing of the experimental apparatus.

simulation of the entire beamline reaction chain from electron beam to photon beam to separated  $e^+e^-$  pairs. A closeup of the magnet and converter region is shown in Fig. 6.

The process of making a secondary beam always presents issues of secondary beam quality and rate, and primary beam power deposit. In this case, more  $e^+e^-$  pairs are created for 1) higher electron beam current, 2) thicker radiators, and 3) thicker converters. The latter two have been made as thick as possible without introducing degradation of the secondary beam quality due to secondary interactions, such as multiple scattering in the radiator or bremsstrahlung in the converter. Those limits will be studied in detail for the full proposal; for now, reasonably conservative values have been chosen:  $10^{-3}X_0$  for the radiator,  $10^{-2}X_0$  for the converter. Having made those choices, the limiting factor is the power deposit in the tagger beam dump, which has several limits. All operating experience with the tagger dump has been constrained to the limit of 800 watts. At 5.5 GeV, this results in a current limit of 145 nanoamperes. These are the limits for the tagger

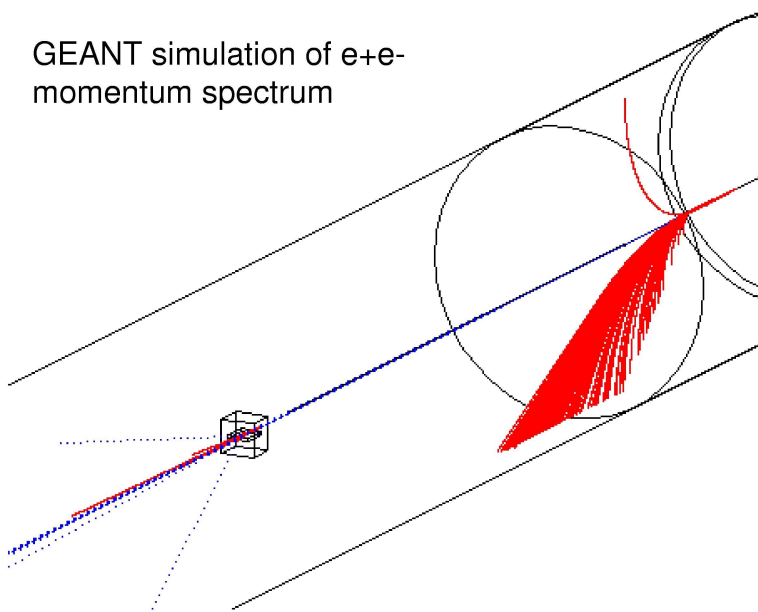


Figure 5: A schematic drawing of the experimental apparatus from a GEANT simulation.

dump in its present configuration, however, the dump was designed for an ultimate limit of 10 kilowatts. This power deposit is feasible if air cooling is added to the dump. The piping for the air cooling was installed at the time of construction. To make use of the higher power limit, an air blower needs to be installed; the design radiological impact on groundwater should be confirmed; a scheme for handling the exhaust air should be conceived and implemented; and the dump temperature should be monitored. These are all straightforward steps. At 5.5 GeV, the 10 kW limit corresponds to 1.8 microamperes. Since this is more than an order of magnitude more current than has ever been tried, for this letter of intent a 1.0 microampere limit has been assumed.

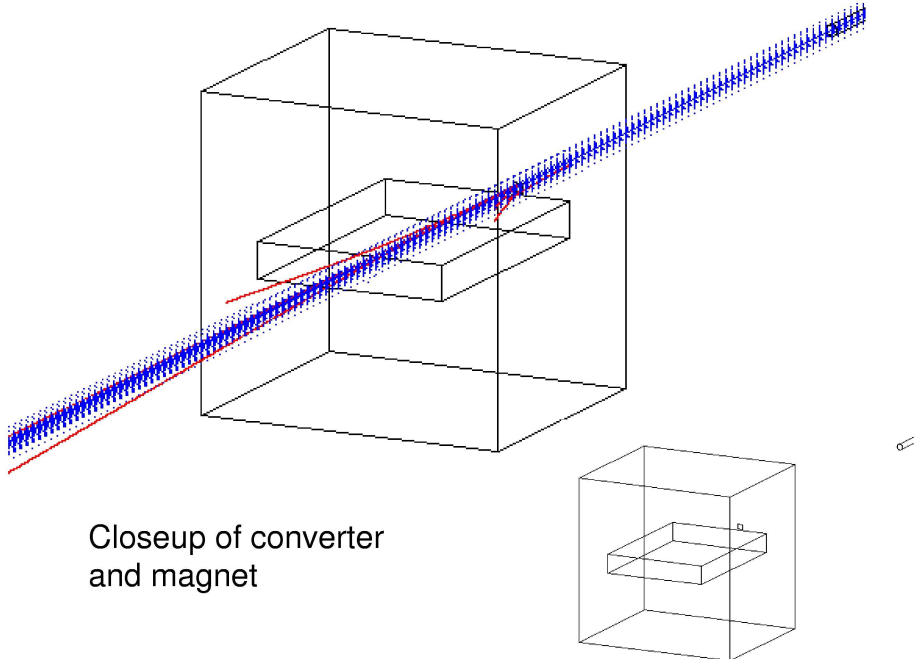


Figure 6: Closeup view of the magnet and converter from the GEANT simulation.

### 3.2 Triggering and data analysis

The usual single-electron trigger employed by CLAS is not appropriate for this measurement; this trigger, based on the Cerenkov counter and electromagnetic shower calorimeter, would miss electrons and positrons at larger angles, severely limiting the coverage in  $\epsilon$ . A further reason not to use the conventional trigger is that it may be biased by the Cerenkov counter, since that device has a slightly different efficiency for outbending and inbending tracks.

Instead, a trigger that selects two charged tracks in opposite sectors will be constructed by requiring hits in time-of-flight counters in opposite sectors in addition to a Level 2 (drift chamber) trigger in the same sectors. Other

prescaled triggers may also be useful. The standard CLAS trigger system is adequate to fulfill these requirements.

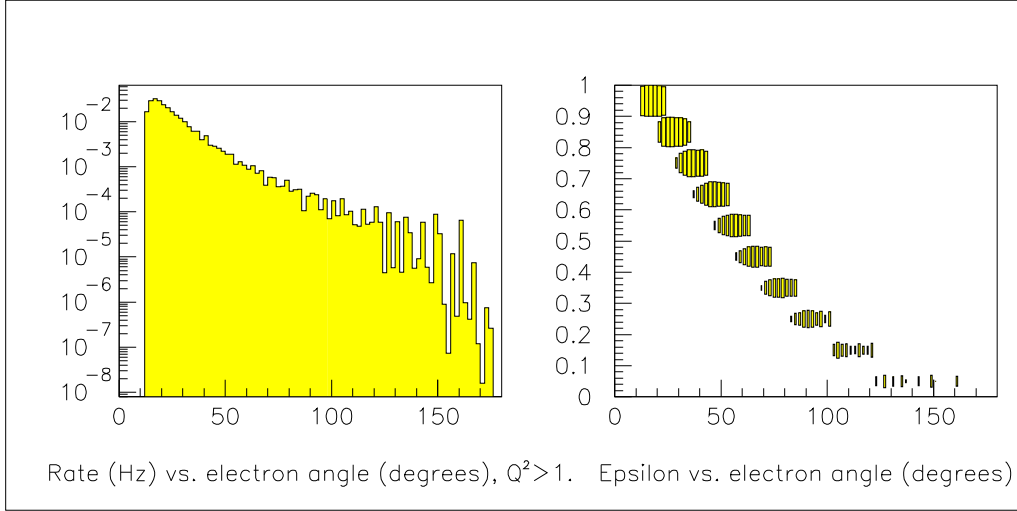


Figure 7: Rates for elastic electron scattering for  $Q^2 > 1 \text{ GeV}^2$  in the left panel; note the large angles of the electrons for small epsilon, which imposes a cutoff of approximately 0.1 in epsilon. The correlation between epsilon and electron angle is shown in the right panel (the right panel has a logarithmic “z” axis).

It may be advantageous to employ a ‘start counter’ in the trigger as well, that is, a thin scintillator-based detector surrounding the target area. A start counter has been used for nearly all photon beam experiments in CLAS. While inducing additional multiple scattering, it has the advantage that it allows measurement of the time-of-flight of each particle that is detected by the time-of-flight counters that surround the drift chambers.

Because the secondary beam current is low, the singles rates will be lower than for ordinary CLAS operation with a few nanoampere electron beam. This means it will be feasible to employ a less restrictive trigger than would be possible for normal beam operations.

In an ordinary electron scattering experiment, the beam energy is fixed. However, for the proposed measurement, the positron and electron beams have a dramatically varying energy due to the  $1/E_\gamma$  energy spectrum convoluted with the  $e^+e^-$  pair production energy distribution. Therefore, the

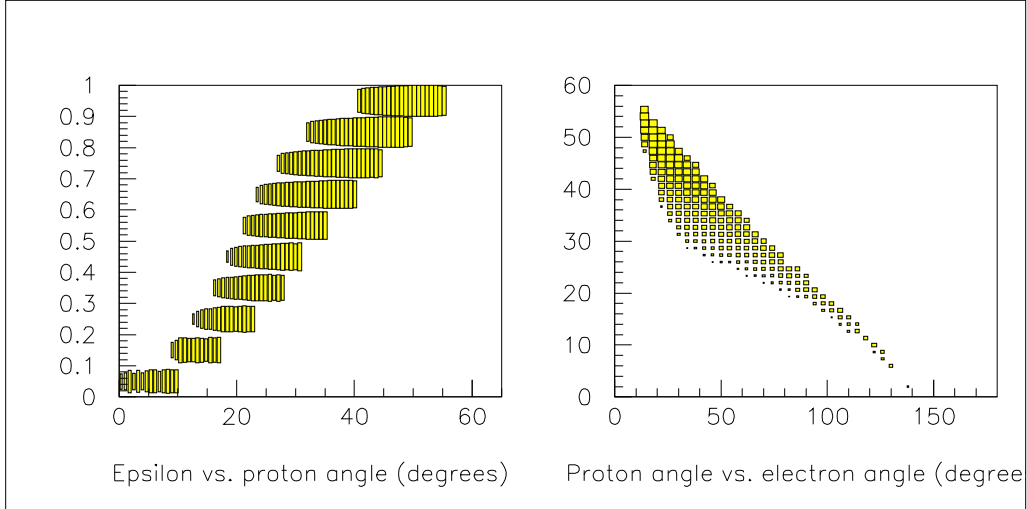


Figure 8: In the left panel is shown the correlation between epsilon and the proton angle; as in Fig. 7, the lower limit of epsilon is approximately 0.1 due to the proton acceptance in CLAS for normal torus polarity, and will be somewhat higher for reversed field conditions. The right panel shows the correlation between the proton angle and the electron angle. Both plots have logarithmic “z” axes.

‘beam energy’ (incident lepton energy) and the value of  $\epsilon$  vary event-by-event.

The elastic scattering process is highly overconstrained if the momentum vectors of both identified final state particles are measured. Therefore, for this reaction the incident lepton energy can be determined event-by-event. For more complex final states such as single pion production, this determination can also be performed as long as all final state particles are measured. This may be useful for understanding backgrounds in the data as well as for other types of experiments comparing positron-induced and electron-induced reactions.

The analysis method can be considered in two possible scenarios, depending on whether a start counter is used or not. With the present instrumentation, the start counter and the minitorus cannot simultaneously be used because of space limitations. A smaller start counter could solve this conflict if necessary.

Without the start counter, the analysis chain would proceed as follows.

The first criteria to be applied is to select events with only two hit-based tracks. The next requirement, that the tracks be co-planar and in opposite sectors, will strongly favor elastic scattering. Assigning particle #1 to the lepton and particle #2 to the proton as a hypothesis, one can calculate the vertex time difference between the two tracks; using the alternate hypothesis with particle #1 as proton and #2 as lepton, one can again calculate the vertex time difference; the correct vertex time difference will be consistent with zero. The resolution should be more than adequate to identify the lepton of the pair using this method. In addition,  $dE/dx$  in the time of flight counters (comparing to the momentum from hit-based tracking) can provide further information to help identify the proton.

Once the lepton is identified, its vertex time can be used to provide an event start time for time-based tracking. The proton identification can be validated by calculating its mass from the time of flight and momentum. The incident lepton energy can be calculated from the lepton and proton variables.

If the start counter is present, the analysis is slightly simplified in that the particle mass can be calculated from the time of flight and the momentum from hit-based tracking. The fastest particle in each event can be used to perform time-based tracking. In this case, a more general analysis can be performed, including limited analyses of other final states such as single pion production. The opposite sector co-planarity requirements for elastic scattering can then be performed with the improved resolution from time-based tracking, and the analysis proceeds as above.

Plots showing the kinematic correlations for the proposed measurement are given in Figures 7 and 8.

### 3.3 Systematic errors

The purpose of the experiment is to precisely compare the  $e^+p$  differential cross section to the  $e^-p$  differential cross section. A short list of the potential sources of systematic error:

1. differences in the determination of the electron and positron momentum vector
2. differences in the acceptance of the electrons and positrons

3. differences in the determination of the momentum vector of the protons from the two reactions
4. differences in the acceptance of the protons from the two reactions
5. differences in the positron and electron incident flux
6. differences in the density and length of the two hydrogen targets
7. differences in the radiative corrections for the two reactions

Two powerful approaches to addressing these issues are to reverse the magnetic field in the separator magnet, and to reverse the torus magnetic field. The former interchanges the incident electrons and positrons, and the latter interchanges the scattered electrons and positrons.

Reversing the field in the separator magnet interchanges the incident electron beam with the positron beam. To the extent that the magnet pole faces are uniform over the small volume of interest, and the field values are reproducible, and that there are no other magnetic fields affecting their trajectories, the electrons and positrons will follow exactly the same path when the separator field is reversed. They will enter the hydrogen targets in exactly the same locations. Averaging the data taken with the two separator field polarities will average out any differences in target length and density, even if the angle of the incident photon beam is not perfectly aligned. Frequent changes of the polarity will average out slowly varying time-dependent problems, such as 'dead wires' that may develop in the drift chambers.

A second benefit from interchanging the incident leptons is that the proton acceptances and reconstruction efficiencies will be identical if the data from the two polarities are averaged. Because the targets will be close to the beamline, the proton acceptances are nearly identical to begin with, but the averaging will remove any remaining subtle effects. This will also permit use of longer targets, thereby increasing the event rate.

The third benefit from interchanging the incident leptons is that the proton momentum vectors are measured in identical regions of the detector, and therefore any systematic errors in their measurement are common to both reactions. As a result, cuts on the proton variables will have an identical effect on the  $e^+p$  and  $e^-p$  yields. Because of this advantage, in the analysis the reaction can be defined by the proton, with only loose cuts on the electron and positron variables. In this way, systematic errors on the measurement of

the electron and positron momentum vectors have a minimal effect. For instance, a calculation of  $W$  using the lepton variables only has to be accurate enough to distinguish elastic scattering from inelastic scattering. The only residual effect of systematic differences between the positron and electron variables is in the determination of the incident lepton energy. Because the kinematics is overdetermined, there are several cross-checks that can be used to study this, and in addition it can be corrected as in the following section.

Turning now to the effect of reversing the torus field, this change has the effect of interchanging the scattered electrons and positrons. The positron acceptance now is identical to the electron acceptance before changing the field, and any systematic errors in the positron variables are the same as those of the electron in the former condition. The only exception to this statement is for time-dependent problems with characteristic times of less than few hours, which is the time required to reverse the polarity. An example might be the development of inefficient detector channels. While these problems tend to persist for much more than a few hours, in any case the residual impact of dead channels developing during the run can be simulated.

Determination of the incident lepton flux is not directly addressed by changing magnetic fields. Only the ratio of fluxes in a given energy bin is needed. The primary way this will be addressed will be by calculation and detailed simulation. It may also be possible to measure the flux in a given energy bin directly by reducing the beam current and using a high field setting on the separator magnet, then count the rate in position-sensitive devices such as small scintillators, a drift chamber, a silicon strip detector, or CLAS itself. Using this method will require a precise determination of the incident photon beam direction relative to the location of the position-sensitive device. It may be of benefit to provide for rotation of the magnet or the position-sensitive device through 180 degrees to provide an additional cross-check.

In summary, the residual errors are likely to be the following:

- an incorrect assignment of  $Q^2$  due to systematic errors in the measurement of the proton kinematic variables and errors in the determination of the incident lepton energy. This is of little consequence if the ratio  $e^+p/e^-p$  is used, since the function varies slowly with  $Q^2$ .
- the effect of detector channels changing characteristics on a timescale of less than a few hours, so that reversing the torus field does not give

identical acceptances and efficiencies for the leptons. This can be simulated; CLAS absolute acceptances can be simulated with an accuracy of approximately 5%, as has been shown by studies of elastic scattering. If the *ratio* of positron and electron acceptances is calculated, the error should be significantly smaller, because the two calculations have strongly correlated errors. Alternatively, careful checking for changing conditions and eliminating data for periods of unstable operation is another approach to limit this error. Given these two considerations, the error should be well-controlled and small.

- the ratio of the incident lepton fluxes will be calculated and simulated, and directly measured as part of the experiment.
- the effect of the difference in the QED radiative corrections between the two processes is estimated to be zero in the relative yields in a given bin, but there could in principle be a very small bin centroid shift.

In conclusion, we believe that the systematic errors can be controlled to approximately the 1% level because of the uniquely symmetric nature of the interaction under study, in combination with the large angle and momentum acceptance of CLAS. More detailed studies are needed to define a precise number.

### 3.4 Rate estimate

The 'beam' of positrons and electrons obtained from the apparatus has a wide range of energies. The rate estimate has been obtained by integrating the elastic scattering rate over the energy profile of the incident leptons. The lepton energy profile has been calculated using a GEANT simulation of the entire beamline apparatus, starting with a 5.5 GeV electron beam.

The event rate as a function of  $Q^2$  is given by

$$\frac{dR}{dQ^2}(Q^2) = \int_E \frac{d\mathcal{L}^{e^+e^-}}{dE}(E) \cdot \frac{d\sigma}{dQ^2}(Q^2, E) \cdot dE \quad (6)$$

where  $E$  is the incident lepton energy and  $\frac{d\mathcal{L}^{e^+e^-}}{dE}(E)$  is the energy-dependent luminosity of the incident leptons. The latter term can be expressed as the product of the target thickness  $t$  and the energy-dependent lepton current  $I(E)$ :

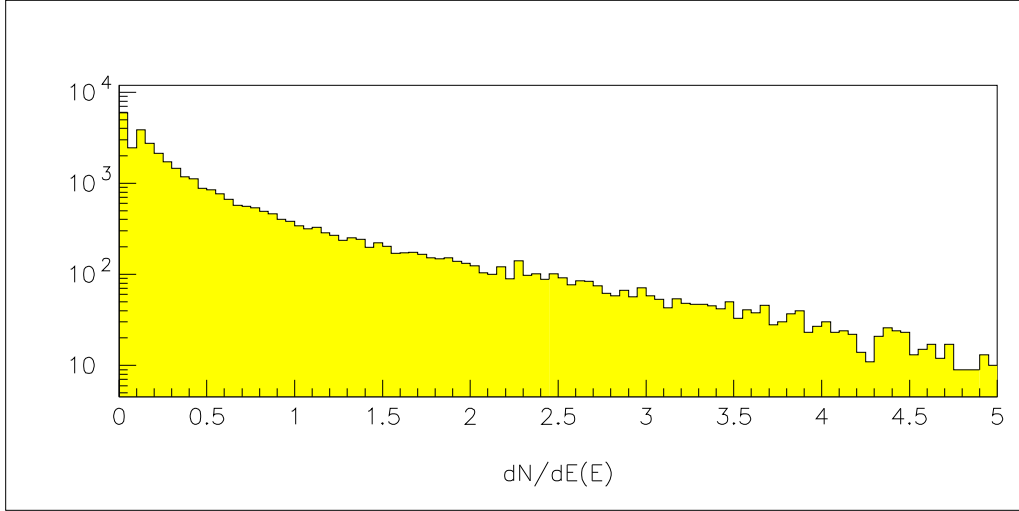


Figure 9: Profile of  $\frac{dN^{e^+e^-}}{dE}(E)$  vs. lepton energy  $E$  from the GEANT simulation.

$$\frac{d\mathcal{L}^{e^+e^-}}{dE}(E) = t \cdot \frac{dI}{dE}(E) = t \cdot c' \cdot \frac{dN^{e^+e^-}}{dE}(E) \quad (7)$$

where  $c'$  is the ratio of the desired beam current passing through the radiator to the total number of thrown events in the simulation. Putting it all together,

$$\frac{dR}{dQ^2}(Q^2) = c \cdot \int_E \frac{dN^{e^+e^-}}{dE}(E) \cdot \frac{d\sigma}{dQ^2}(Q^2, E) \cdot dE \quad (8)$$

where  $c = 0.0000087/\text{GeV}^2 \cdot s$  for a 20 cm long hydrogen target of density  $0.071 \text{ g/cm}^3$ , 1000 nanoamperes of beam incident on the tagger, a radiator of  $10^{-3}$  radiation lengths, a converter of  $10^{-2}$  radiation lengths, an average acceptance of 0.4, and 40 million thrown electrons. The first term under the integral,  $\frac{dN^{e^+e^-}}{dE}(E)$ , comes from the GEANT simulation and is shown in Fig 9. The second term is calculated using dipole form factors. The integration is performed numerically.

The rates thus obtained are shown in Fig. 10; the electron singles rate with  $Q^2 > 1 \text{ GeV}^2$  was shown previously in Fig. 7. While the rates for

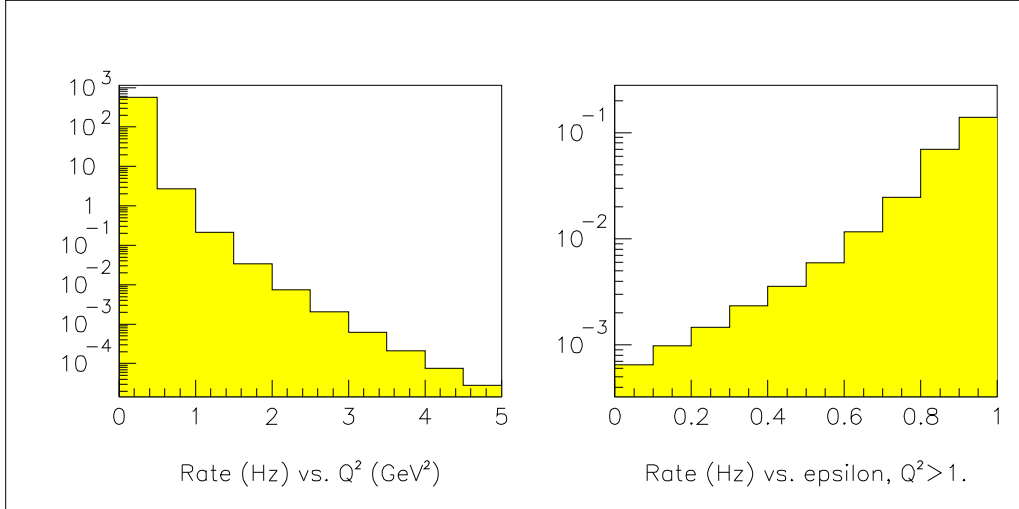


Figure 10: The rate of elastic scattering events as a function of  $Q^2$  (left panel) and  $\epsilon$  (right panel). The right panel has the requirement  $Q^2 > 1 \text{ GeV}^2$  applied.

small epsilon are lower, they are still measurable within practical beamtime constraints.

## 4 Anticipated Beam Request

The running conditions and anticipated beam request are shown in Table 1. The conditions selected are based on best known practices, GEANT simulation, and cryotarget technology that is known to be achievable. The limiting statistical error is for smallest epsilon. An average acceptance of 0.4 is assumed for all the data, based on experience with elastic and quasi-elastic scattering experiments performed in CLAS. The total number of PAC days required is 29, which allows for 3 days of lepton flux measurements and several torus polarity changes, which require approximately half a shift each.

A plot of the expected data quality is shown in Fig. 11. This may be compared with the data of Fig. 2 which are shown on the same vertical axis range. A very significant improvement in our understanding of the epsilon dependence of this ratio would clearly be obtained from the CLAS

Table 1: Anticipated running conditions, statistical accuracy for low-rate bins, and anticipated beamtime request.

Item	Value
Radiator thickness	$10^{-3} X_o$
Converter thickness	$10^{-2} X_o$
Cryogenic hydrogen target length	20 cm
Tagger current	$1 \mu A$
Beam energy	5.5 GeV
Torus current	750 A
Average acceptance assumed	0.4
Tagger current	$1 \mu A$
Full bin width in $\epsilon$	0.1
PAC days for data acquisition	26
Statistical error, $\epsilon = 0.15 \pm 0.05$	2.1%
Statistical error, $\epsilon = 0.55 \pm 0.05$	0.86%
Additional days for flux measurement and torus polarity changes	3

data. This would in turn greatly strengthen our understanding of the role of the two-photon exchange in the elastic scattering process, and may resolve the currently dilemma concerning the discrepancy between the Rosenbluth-method analysis and the polarization analysis.

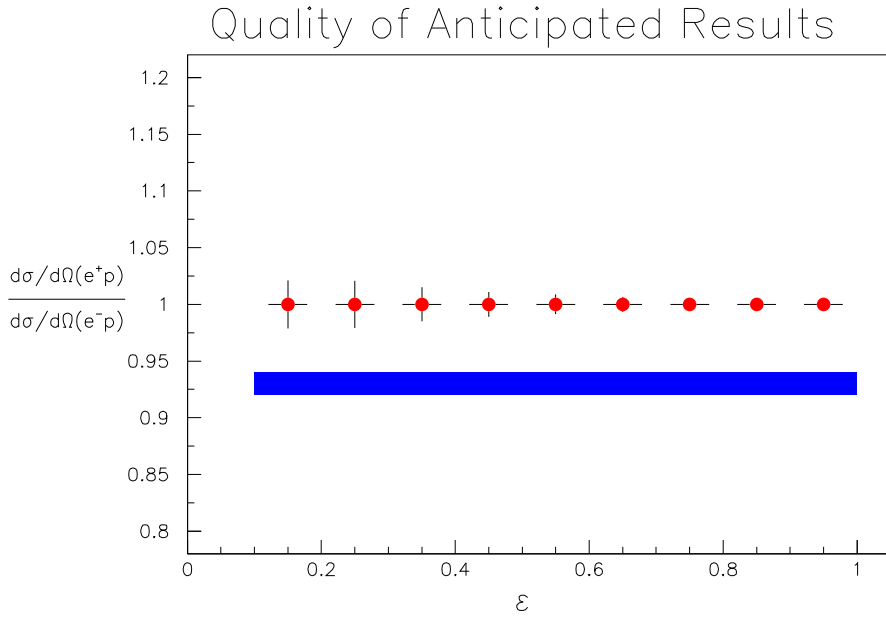


Figure 11: A plot of the expected experimental uncertainties. The systematic error is indicated by the bar below the data points, while the errors on the points indicate the statistical uncertainty.

## References

- [1] L. Andivahis *et al.*, Phys. Rev. D **50** (1994) 5491.
- [2] M.K. Jones *et al.*, Phys. Rev. Lett. **84** (2000) 1398.
- [3] O. Gayou *et al.*, Phys. Rev. Lett. **88** (2002) 092301.
- [4] J. Arrington, nucl-ex/0305009.
- [5] M.C. Christy *et al.*, to be submitted to Phys. Rev. C.
- [6] P.A.M. Guichon and M. Vanderhaeghen, Phys. Rev. Lett. **91** (2003) 142303.
- [7] P. Blunden, W. Melnitchouk and J. Tjon, Phys. Rev. Lett. **91** (2003) 142304.

- [8] A. Afanasev, S. Brodsky and C. Carlson, presented by A. Afanasev at the DNP Meeting, Tucson, AZ, Oct. 2003.
- [9] Y.S.Tsai, Phys. Rev. **122**, 1898 (1961), L.W. Mo, Y.S. Tsai, Rev. Mod. Phys. 41, 205 (1969).
- [10] E. Offerman *et al.*, Phys. Rev. C **44** (1991) 1096.
- [11] Fricke *et al.*, Phys. Rev. C **45** (1992) 80.
- [12] Voegler *et al.*, Phys. Rev. C **43** (1991) 2172.
- [13] Gueye *et al.*, Phys. Rev. C **57** (1998) 2107.
- [14] J. Arrington, nucl-ex/0311019.
- [15] M.N.Rosenbluth, Phys.Rev. **79**, 615 (1950).
- [16] L. C. Maximon and J. A. Tjon, Phys. Rev. C **62**, 054320 (2000).
- [17] A. Afanasev, I. Akushevich and N. Merenkov, Phys. Rev. D **64**, 113009 (2001); A. V. Afanasev, I. Akushevich, A. Ilyichev and N. P. Merenkov, Phys. Lett. B **514**, 269 (2001).
- [18] J. Mar *et al.*, Phys. Rev. Lett. **21**, 482 (1968).
- [19] S. D. Drell and J. D. Sullivan, Phys. Lett. **19**, 516 (1965).